ISSN 2411-3336; e-ISSN 2541-9404

JOURNAL OF MINING INSTITUTE

Zapiski Gornogo instituta

Journal homepage: pmi.spmi.ru



Research article

Garnetites from Marun-Keu eclogite complex (Polar Urals): geochemistry and the problem of genesis

Laysan I. SALIMGARAEVA[1,2]✉, **Alexei V. BEREZIN**[1,3]

[1] *Institute of Precambrian Geology and Geochronology RAS, Saint Petersburg, Russia*

[2] *The Zavaritsky Institute of Geology and Geochemistry, Ural Branch of the RAS, Ekaterinburg, Russia*

[3] *Institute of Earth Sciences, Saint Petersburg State University, Saint Petersburg, Russia*

***How to cite this article*:** Salimgaraeva L.I., Berezin A.V. Garnetites from Marun-Keu eclogite complex (Polar Urals): geochemistry and the problem of genesis. Journal of Mining Institute. 2023. Vol. 262, p. 509-525. EDN CLAFSR

Abstract. A comprehensive mineralogical and geochemical characterization (XRF, ICP-MS, SEM-EDS, SIMS methods) of garnetites and their protoliths from the Marun-Keu complex (Polar Urals), one of the key objects in understanding the evolution of the Uralian Orogen, is presented. Garnetites and their protoliths from the Marun-Keu complex, Polar Urals, a key locality for understanding the evolution of the Uralian Orogen, are described mineralogically and geochemically using XRF, ICP-MS, SEM-EDS and SIMS methods. Ultramafic (in most cases) and mafic rocks are understood as protoliths for garnetites. A general trend for garnetites is an increase in total REE concentration relative to that of their protoliths. All the analyzed garnetites display a considerable decrease in Cr, Ni and Co. V concentration in the garnetites is also lower than that of the protoliths, though not so markedly. Garnets from garnetites evolving after peridotites generally exhibit elevated (relative to garnets from garnetites evolving after mafic rocks, such as porphyrites) Prp and lowered Alm content, which seems to be due to high Mg concentration in the protolith. In garnetites after peridotites a garnet exhibiting an uncommon non-differentiated REE spectrum with a considerable positive Eu-anomaly was found, which could be due to the inheritance of a REE spectrum by garnet from a precursor mineral, in this case plagioclase. Slyudyanaya Gorka garnetites were probably formed from mafic and ultramafic rocks in oceanic crust, which migrated to higher levels of the section under the influence of the crustal fluid flowing along fracturing zones.

***Keywords*:** garnetites; eclogites; garnets; trace elements; rare earth elements; Marun-Keu complex

Acknowledgment. The study was financially supported by RSF N 22-17-00177.

Received: 03.12.2022 ***Accepted: 23.03.2023*** ***Online: 23.06.2023*** ***Published: 28.08.2023***

Introduction. Garnetites (rocks with at least 50 % garnet) often occur in metamorphic complexes [1-3]. Experiments confirm that eclogites were completely metamorphosed into garnetites at pressures of about 15 gPa upon oceanic crust subduction [4-6]. Garnetites have also been found among granulites in the shear-zones of the Khabarninsk mafic-ultramafic massif, Southern Urals [7] and in the Condalite Belt of the North China Craton [8]. They are characteristic of the giant Broken Hill deposit produced by granulite-facies metamorphism and the active contribution of fluids [9, 10].

The origin of garnetites has long been the subject of active discussion. Many authors believe that garnetites were produced by the metamorphism of primarily differentiated igneous rocks [11]. Others think that garnetites are a result of metamorphic differentiation supported by active fluid infiltration [3] and metasomatism with a formation of a metasomatic column [12]. Garnet with a high spessartine content may often be produced by the metamorphism of Fe- and Mn-enriched sediments [13]. In many hypotheses, a considerable amount of fluids, responsible for the mobility of some components, is involved in garnetite formation [14, 15].

This is an open access article under the CC BY 4.0 license

In the northwestern Belomorian Mobile Belt, the large-scale garnetization of eclogite bodies, leading to the formation of monomineral garnetites, was revealed in Salmi eclogites dated at ca. 1900 Ma. The study of an eclogite body in the quarry of the Kuru-Vaara deposit showed that garnetite formation was separated in time from eclogitization but was simultaneous with the intrusion of cross-cutting pegmatite veins about 1840 Ma ago responsible for the addition of LREE and other HFSE (Y, Zr, Hf and Th) [16].

The Marun-Keu eclogite complex located in the Polar Urals is poorly studied. The character of the protoliths and the age and conditions of formation of Marun-Keu eclogites remain the subject of debate [17-19]. Previously, the attempts were made to decipher the metamorphic evolution of Marun-Keu eclogites by the detailed major-element study of garnets with no account for trace and rare earth element (REE) distribution [20, 21]. An abundance of garnetites among Slyudyanaya Gorka eclogites was reported by N.G.Udovkina [22], a pioneer researcher of eclogites in the Polar Urals, but was disregarded in all more recent studies.

The aim of the present study is to analyze the pattern of variations in the major, trace and rare earth element composition of garnets and co-existing minerals from various types of garnetites in the Marun-Keu eclogite complex, as applied to garnetite formation problems. Garnet is a key mineral used to assess metamorphic parameters [23, 24] and to date garnet contenting parageneses by Sm-Nd and Lu-Hf methods [25, 26]. Trace- and rare-earth elements are widely used for assessing geochemical crystallization environments and for studying the conditions of formation of genetically different minerals, such as zircon [27-29], titanite [30], beryl [31-33], olivine [34, 35], etc.

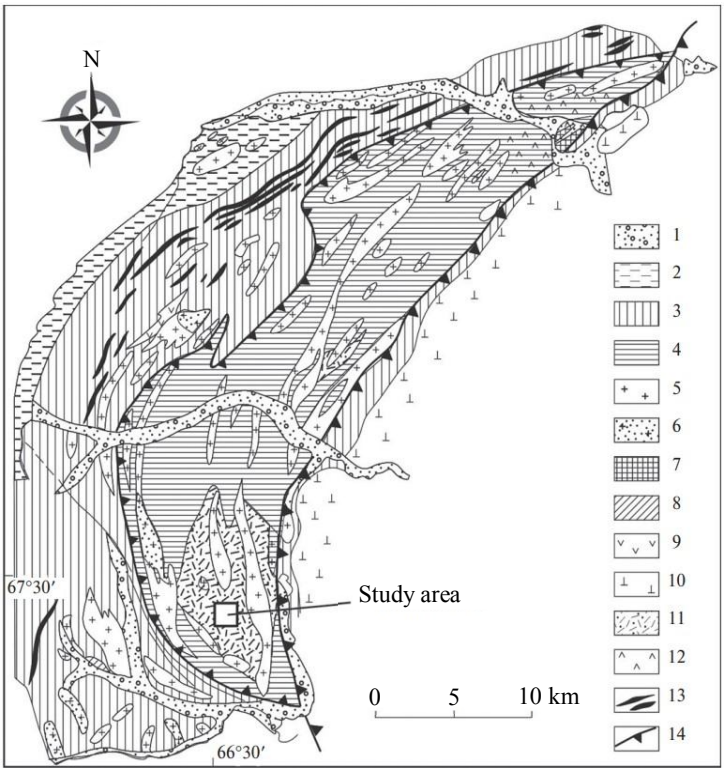


Fig.1. Schematic geological map of the Marun-Keu complex [17, 22]

1 – quartenary sediments; 2 – paleozoic sediments; 3 – Nyaroveiskaya series: quartz-graphite, quartz-sericite, amphibole-chlorite schists, conglomerates, sericite-chlorite schists with interlayers of quartzites, sandstones and marbles, quartz-sericite-chlorite thin-banded schists with interlayers effusives; 4 – Marun-Keu complex: alternation of amphibolites (garnet, albite, micaceous, micaceous-chlorite) with gneisses, granite-gneisses and eclogites; 5 – granites, gneissic granites; 6 – granitic rocks with fluorite; 7 – metarhyolites; 8 – diorites; 9 – gabbroic rocks; 10 – ultramafic rocks (Syum-Keu complex); 11 – eclogites predominating; 12 – occurrence of glaucophane; 13 – quartz-graphite shist; 14 – zones of tectonic faults

Geological description of the study area. The Marun-Keu complex is a key locality in the evolution of the Uralian Orogen. It is a tectonic block, 14×70 km in size, confined to the Main Uralian Fault zone (Fig.1) [22]. Eclogites and the relics of their protoliths are most common in the southern Marun-Keu complex (Slyudyanaya Gorka location). Eclogite exposures are confined to the axial portion of the Marun-Keu complex, where eclogites and their protoliths occur as lenticular blocks in granite-gneiss matrix [22].

The hilltop near elevation mark 1040 (67°28′16.5″ N, 66°29′24″ E) consists of massive ultrabasic rocks. There is a ~10 m thick schistosity zone in ultrabasic rocks on a south-facing slope. The zone dips subvertically and has a strike azimuth of 340°. It contains eclogite lenses conformal to it (Fig.2, *a*). The lenses strike for over 15 m and increase in thickness from 0.2 to 5 m from the

This is an open access article under the CC BY 4.0 license

Journal of Mining Institute. 2023. Vol. 262. P. 509-525
© Laysan I. Salimgaraeva, Alexei V. Berezin, 2023

base to the top of the exposure. They contain scarce ~5 cm thick granitite aggregates confined to contacts with ultrabasic rocks (sample 2204, Fig.2, *b*). Two garnetite samples were taken downslope from eluvial boulder scree 200 m SW (samples 2224 and 2225).

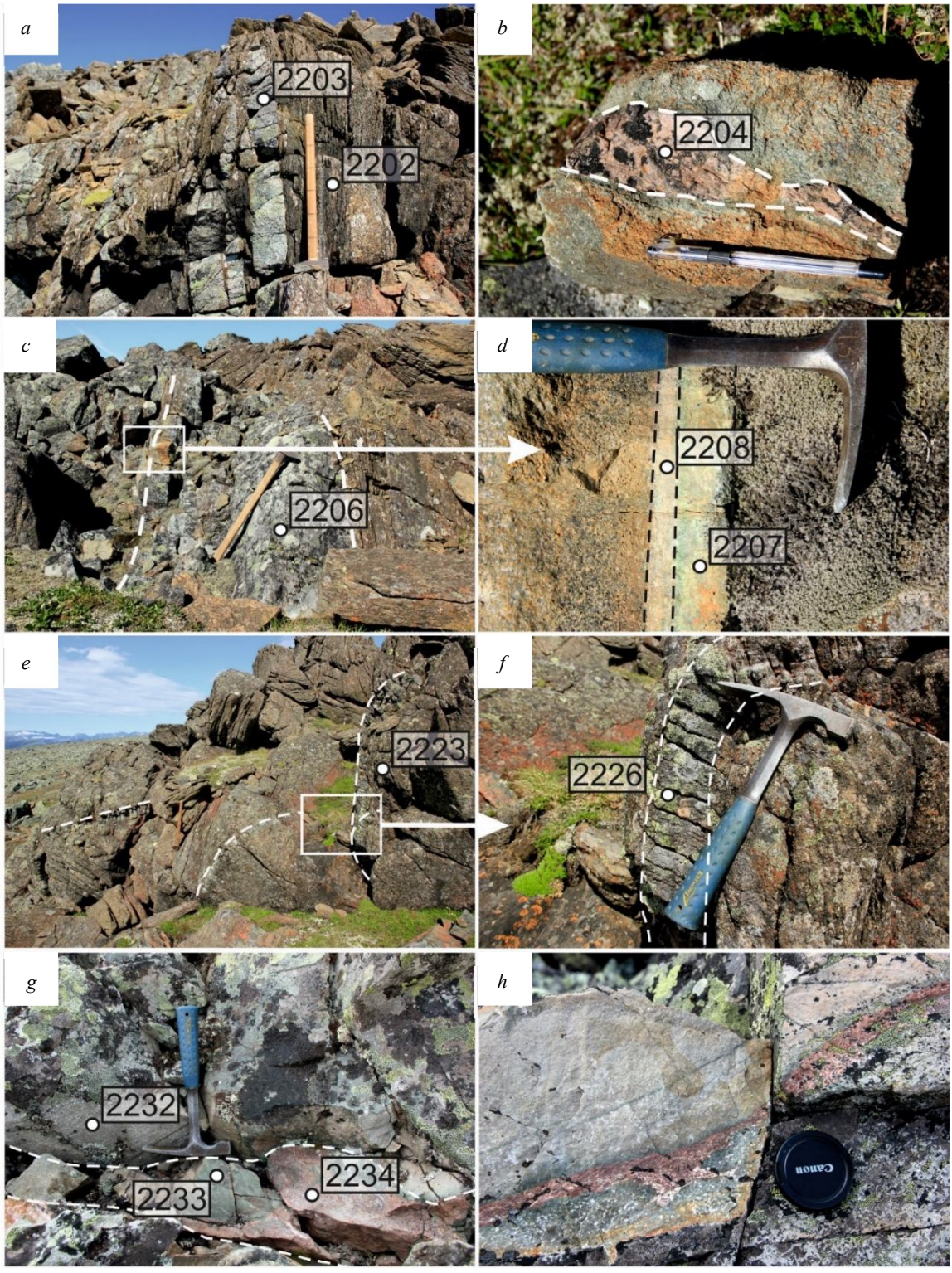


Fig.2. Photographs of exposures: *a* – lenses of eclogites in the zone of shearing of ultramafic rocks; *b* – separation of garnete in eclogite; *c* – eclogite lens in the ultramafic shear-zone; *d* – metasomatic column at the contact ultramafic (left) and eclogite (right); *e* – massive ultramafic rocks with multidirectional veinlets garnetites (white dotted line); *f* – veinlet of garnetite with amphibolization zones; *g*, *h* – garnetite development zones and eclogites in porphyrites

This is an open access article under the CC BY 4.0 license

Metasomatic zoning (Fig.2, *d*), occurring as a garnetite zone (sample 2208) and a zone of chlorite-amphibole epidote composition complementary to it (sample 2207), evolves locally at the contact of eclogite lenses with ultrabasic host rocks (Fig.2, *c*). The total thickness of the metasomatic column is no more than 5 cm.

500 m SSW of elevation mark 1040 (67°27′49″ N, 66°29′27″ E) is a massive ultrabasic rock exposure. Ultrabasic rocks on the southwestern slope contain garnet, and garnet peridotites gradually transform into amphibolized eclogites. Further upslope, garnet peridotites display numerous multidirectional 2-3 cm thick garnetite veinlets (sample 2226) (Fig.2, *e*) with ~15 cm thick amphibolization zones on each side (Fig.2, *f*).

At 300 m east of the above exposure (67°27′50″ N, 66°29′55″ E) there is a serrate remnant consisting of mafic porphyrites, after which fine-grained eclogites and garnetization zones evolve. The zones (sample 2234) vary in thickness from a few centimeters to tens of centimeter veinlets (Fig.2, *g*). Occurring at garnetite-host porphyrite contacts are ~1 cm thick amphibolization rims (Fig.2, *h*).

It is shown that two rock varieties, ultrabasic and basic rocks, are protoliths for garnetites. All basic rock varieties are described in detail in [22]. Let us discuss some of their important characteristics.

One type of a protolith for garnetites is ultrabasic rocks. Macroscopically (sample 2202, Fig.3, *a*, *b*), they occur as dark-green to black rocks composed mainly of olivine with minor orthopyroxene. The petrographic study of the rocks shows that they consist mainly of coarse olivine and orthopyroxene grains. The olivine grains (up to 90 vol.%) are largely altered to iddingsite-talc aggregate associated with magnetite. Orthopyroxene (up to 2 vol.%), occurring as idiomorphic grains, displays solid solution decay structures in the form of thin lamellae. Pyroxene is often replaced by colourless chlorite aggregate (Fig.3, *a*, *b*). Xenomorphic garnet occurring in the rock (up to 10 vol.%) is highly altered on its margin, forming granular high-Mg chlorite aggregate. Thus, based on its mineral composition, it can be identified as a garnetiferous ultrabasic rock (peridotite [22]).

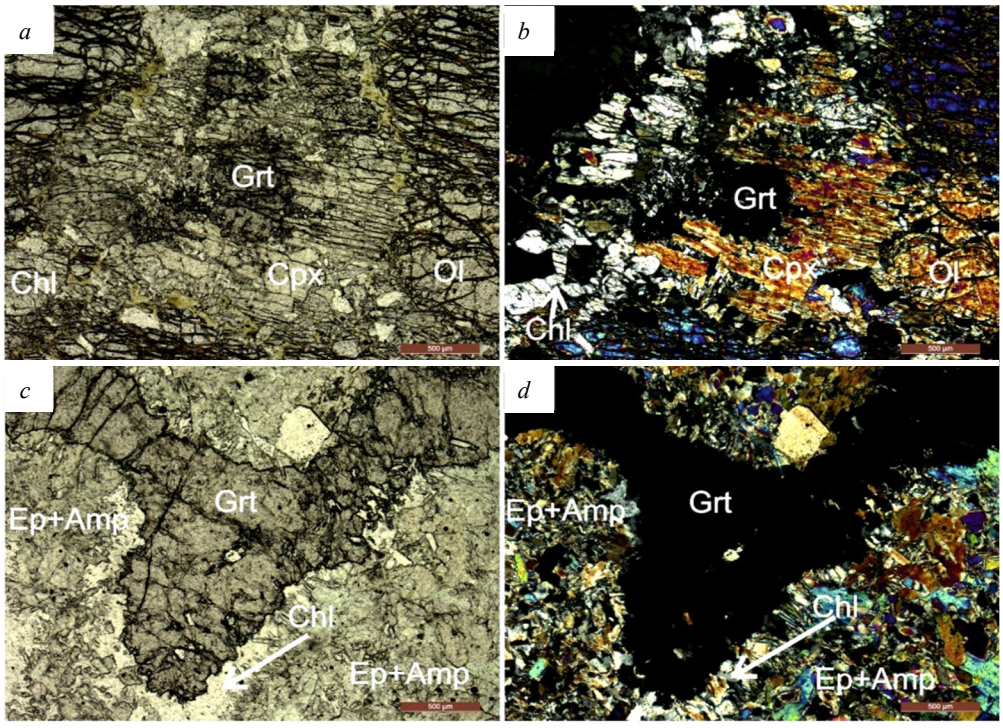


Fig.3. Photo of thin sections: garnet peridotite (sample 2202) without an analyzer (*a*), with analyzer (*b*); eclogite (sample 2203) without analyzer (*c*), with analyzer (*d*)

This is an open access article under the CC BY 4.0 license

Journal of Mining Institute. 2023. Vol. 262. P. 509-525
© Laysan I. Salimgaraeva, Alexei V. Berezin, 2023

Upon the metamorphism of peridotite (sample 2203, Fig.3, *c*, *d*), the rock clearly preserves the relics of the primary structure up to the complete replacement of olivine and pyroxene. Relics of orthopyroxene are replaced by newly-formed clinopyroxene, colourless amphibole and chlorite. Genetically more recent garnet aggregates fill interstices between replaced pyroxene and olivine grains, scarcely forming separate fine grains. With these characteristics in view, the rock may be identified as highly altered eclogite.

The other rock type, from which garnetites evolved, is pyroxene basaltic porphyrite (sample 2232). It has been found only at one locality. It is a grey-green rock with fine-grained matrix. Macroscopic study shows that it contains altered plagioclase microliths. The general rock tissue consists of fine-grained aggregate of garnet, amphibole, chlorite, altered plagioclase, and pyroxene. Relics of phenocrysts occur as colourless chlorite pseudomorphs evolving after clinopyroxene. The rock contains up to 3 vol.% rutile of metamorphic origin. The above characteristics suggest that the rock can be attributed to pyroxene porphyrite of the basic composition.

Upon the formation of eclogite after porphyrite (sample 2233), garnetization becomes more vigorously, filling the matrix with xenomorphic aggregates without faceted grain formation. The coarsest (up to 300 μm) garnet aggregates contain colourless chlorite inclusions. Primarily magmatic clinopyroxene grains are replaced by fine-grained metamorphic clinopyroxene aggregate often associated with colourless amphibole. Thus, the rock is identified as an eclogitized porphyrite of the basic composition.

The maximum temperature of formation of these parageneses seems to be no more than 550 °C due to the presence of chlorite, serpentine and mainly colourless amphibole. It has been found [22] that the contacts of eclogitized rock blocks with plagiogranites occur as schistosity zones. Foliated two-mica plagiogranites associated with basic-ultrabasic rocks display one mineral paragenesis with epidote, which is consistent with the above temperature value.

Thus, Slyudyanaya Gorka garnetites can be divided into several types: garnetites associated with eclogites (as xenomorphic lenticular aggregates in eclogite bodies and as a constituent of metasomatically formed zones at the ultrabasic rock-eclogite contact); thin (no more than 5 cm) monomineral veins cutting ultrabasic rock blocks (a rarer type). Field studies show that the formation of vein-hosting fractures was affected by brittle-ductile rock deformations.

Analytical methods. Major element composition in the rocks were analyzed using a standard X-ray spectral fluorescence method (XRF) on an ARL-9800 multi-channel spectrometer (VSEGEI). The lower determination limit of petrogenic element oxides is 0.01-0.05 wt.%.

Bulk analyses of the rocks for trace and rare-earth elements were performed by an inductively coupled plasma mass spectrometry (ICP-MS) method on an ELAN-DRC-6100 quadrupole mass-spectrometer, using a standard technique (VSEGEI) and acid decomposition in an acid mixture ($HF+HNO_3$). The geological standards USGS were used for checking analytical accuracy. The relative determination error for over 70 elements is no more than 5-10 %: less than 5 % for REE and less than 10 % for Rb, Sr, Ba, Nb, Ta, Zr, Hf, U and Th. The lower detection limits vary within 0.01 % for major and 0.005-0.010 ppm for most trace and rare earth elements.

The chemical composition, structure and interaction of minerals were studied using epoxy resin preparations in a back-scattered electron (BSE) regime on a JEOL JSM-6510LA scanning electron microscope with a JED-2200 energy dispersion spectrometer (IPGG RAS). The end-member composition of minerals was calculated using the program Minal 3.0 developed by D.V.Dolivo-Dobrovolsky (IPGG RAS). The program WinEpclas [36] was used to classify epidote-group minerals. Amphibole composition was calculated using IMA's recommendations and a classification scheme approved by IMA [37]. Mineral abbreviations from [38] were used.

This is an open access article under the CC BY 4.0 license

Trace and rare earth element composition in minerals were analyzed by a secondary ion mass-spectrometry (SIMS) method on a Cameca IMS-4f ion microprobe at Valiev IPT RAS (Yaroslavl branch). The trace element measurement error is up to 10 % for concentrations over 1 ppm and up to 20 % for those of 0.1-1 ppm; the detection limit for various elements ranges from 5 to10 ppb. The trace element composition of rock-forming minerals was determined at the same points as that of major elements. When constructing REE distribution spectra, mineral compositions were normalized for CI chondrite [39].

Results. ***Rock composition.*** Garnetites were compared (if possible) with their original rocks (protoliths), such as basic peridotites and porphyrites, as well as eclogites formed after the same protoliths (Table 1).

Table 1

Rock composition by major elements, wt.%

Components	Garnetites and their protoliths associated with peridotites							Garnetites and their protoliths associated with porphyrites		
	Peridotite	Altered eclogite	Garnetite	Eclogite	Garnetite	Garnet peridotite	Garnetite	Porphyrite	Eclogite	Garnetite
	2202	2203	2204	2206	2208	2223	2226	2232	2233	2234
SiO_2	39.22	39.94	38.06	40.01	40.68	40.66	45.16	48.46	48.44	41.59
Al_2O_3	7.30	18.83	23.04	16.34	22.39	8.35	11.01	17.26	14.87	20.56
TiO_2	0.05	0.04	0.03	0.05	0.02	0.14	0.36	0.49	0.61	3.36
Fe_2O_3t	10.91	8.41	13.21	7.83	9.35	13.27	11.34	10.44	12.23	21.40
MnO	0.16	0.14	0.34	0.12	0.18	0.20	0.32	0.19	0.21	0.22
MgO	34.33	21.43	15.97	22.34	16.71	29.42	19.32	8.54	8.87	2.38
CaO	4.29	9.28	10.30	10.12	10.66	5.07	12.60	12.70	12.29	8.59
Na_2O	< 0.1	0.46	< 0.1	0.32	< 0.1	0.16	< 0.1	1.58	1.62	1.41
K_2O	0.03	0.06	< 0.01	0.05	0.01	0.20	< 0.01	0.17	0.17	0.39
P_2O_5	< 0.05	< 0.05	< 0.05	< 0.05	< 0.05	< 0.05	0.11	0.08	0.09	0.47
LOI	3.81	1.64	0.30	2.00	0.49	1.85	0.17	< 0.1	0.13	< 0.1
Total	100.00	100.00	101.00	99.18	101.00	99.31	100.00	99.99	99.54	100.00

Note. Fe_2O_3t – total iron; LOI – loss on ignition; sample 2202 is protolith for garnetites 2204 and 2208.

Major elements. The analyzed garnetites are characterized by a relatively narrow range of silica content from 38.06 to 45.16 wt.% (Table 1). Sample 2226 contained a maximum concentration of 45.16 wt.%. Silica in garnetiferous peridotite (sample 2223), from which the granitite evolves, contributes only 40.66 wt.%. Silica in garnetites (samples 2204 and 2208) does not differ the from protolith values. Garnetite (sample 2234) evolving after porphyrite (sample 2232) contains less silica (41.59 wt.%) than porphyrite and eclogite (about 48.5 wt.%).

Alumina concentration in three granitite samples is relatively stable – 20.56-23.04 wt.% (samples 2204, 2208, 2234). In sample 2226 it is much lower – 11.01 wt.%. However, all the garnetites display the same trend: their alumina concentration is higher than that of the protolith.

The TiO_2 concentration in three garnetites (samples 2204, 2208 and 2226) is as low as 0.02-0.36 wt.% and is about the same as in the protolith. The TiO_2 concentration of garnetite after porphyrite (sample 2234) is 3.36 wt.%, which is much higher than that in the protolith (0.49 wt.%).

Garnetite after porphyrite (sample 2234) has an increased content of Fe_2O_3t, equal to 21.40 wt.%, significantly exceeding the value for porphyrite – 10.44 wt.%. The Fe_2O_3t content of other garnetites is similar to that of the protoliths – 9.35-13.21 wt.%.

The MnO content of all the analyzed garnetites is 0.18-0.34 wt.%, differing slightly from that of the protoliths.

This is an open access article under the CC BY 4.0 license

Journal of Mining Institute. 2023. Vol. 262. P. 509-525
© Laysan I. Salimgaraeva, Alexei V. Berezin, 2023

One common trend is a decrease in the MgO content of granitites, as compared to that of the protoliths. MgO for samples 2204, 2208 and 2226 is 15.97-19.32 wt.%, while MgO for the protoliths of these garnetites is 29.42-34.33 wt.%. Garnetite after porphyrite (sample 2234) contains the lowest MgO concentration of 2.38 wt.% correlating with its low concentration (8.54 wt.%) in the protolith.

CaO concentration in samples 2204, 2208 and 2226 varies from 10.30 to12.60 wt.%, being about twice as high as that of the protoliths. Conversely, the CaO concentration of garnetite after porphyrite (sample 2234) decreases to 8.59 wt.%, as compared to 12.70 wt.% for porphyrite.

The alkali (Na and K oxides) content of samples 2204, 2208 and 2226 is below the sensitivity limit of the XRF method (or is slightly higher, as K_2O in sample 2208). Garnetite after porphyrite contains 1.41 wt.% Na_2O and 0.39 wt.% K_2O. These values are comparable with those for the protolith.

P_2O_5 concentration is below the sensitivity limit of the XRF method for samples 2204 and 2208, and is 0.11 wt.% for sample 2226 (it is below the detection limit in the protolith). Garnetite after porphyrite contains more P_2O_5 than the protolith (0.39 and 0.17 wt.%, respectively).

To more correctly compare variations in rock composition (ultrabasic and basic rocks), calculations were made using Bart's oxygen method [40], which assumes an isovolumetric alteration pattern. The relative amount of aluminium in garnetites after ultrabasic rocks was shown to increase by 300 % and in those after in basic porphyrites – by 20 %. The relative Mg concentration of all garnetites decreases by 2-4 times relative to the protolith.

Relative Fe concentration in garnetites after porphyrites increases twice and Ti concentration tenfold, which is indicated petrographically by intensive rutile formation.

For all rock associations it was found that silica is least mobile (relative variations make up no more than 10 %), while titanium (up to 700 rel.%) and the alkalies Na and K (up to 300 rel.%) are most mobile.

If silica is taken as an arbitrarily immobile element, then the composition of the source of the fluids provoking eclogitization and garnetization can be assessed. The authors applied such a model of mixing (protolith-fluid) to make preliminary estimates using element ratios [41]. The results suggest that high-alumina sodium granitoids are a source of fluids.

Trace elements. All the garnetites analyzed display a substantial decrease in Cr concentration relative to that of the protolith. The Cr content of garnetites (samples 2204, 2208 and 2226), for which peridotites are protoliths, is 260-526 ppm (Table 2). Cr concentration in the protoliths is much higher – 1500-3100 ppm. Cr concentration in porphyrite is as low as 263 ppm, while in garnetite after porphyrite (sample 2234) it decreases to 41.6 ppm. Variations in Ni and Co were similar to those in Cr, decreasing in garnetites relative to their protolith.

Cu concentration in samples 2204, 2208 and 2226 varied slightly (33.4-91.3 ppm), as compared with that of the protolith. Comparison of porphyrite and garnetite after it shows an increase in Cu from 97.3 to 158 ppm. Zn concentration correlates with Cu concentration, also reaching a maximum of 296 ppm in granitite after porphyrite.

The amount of V in garnetites decreases less markedly relative to their protolith from 37.4 to 11.3 and 15.2 ppm for samples 2208 and 2204, and from 81.1 to 57.1 ppm for sample 2226. The amount of V in porphyrite (sample 2232) is much greater (374 ppm) than in peridotite, but in garnetite after porphyrite (sample 2234) it also decreases to 253 ppm.

Sc concentration in garnetites varies from 2.86 to 19.4 ppm, remaining either the same as that of the protolith or decreasing.

The behavior of Sr displays no regular pattern. It remains unchanged relative to its protolith in sample 2226, decreases in sample 2204 and increases in sample 2208. Sr concentration for these three garnetites varies from 39.2 to 179 ppm. The growth of Sr for garnetite after porphyrite (sample 2234) is more obvious: 547 ppm in garnetite and 197 ppm in porphyrite. Another large-ion lithophile element, Ba, behaves in a similar manner.

This is an open access article under the CC BY 4.0 license

Table 2

Rock composition by trace elements, ppm

Components	Garnetites and their protoliths associated with peridotites							Garnetites and their protoliths associated with porphyrites		
	Peridotite	Altered eclogite	Garnetite	Eclogite	Garnetite	Garnet peridotite	Garnetite	Porphyrite	Eclogite	Garnetite
	2202	2203	2204	2206	2208	2223	2226	2232	2233	2234
Cr	1500	739	260	897	410	3100	526	263	146	41.6
Ni	1220	668	180	707	391	896	306	56.4	77.9	33.4
Co	120	63.9	62.3	70.2	62.6	98.6	53.1	38.8	47.4	29.1
V	37.4	19.9	15.2	25.6	11.3	81.1	57.1	374	396	253
Sc	12.1	5.69	3.66	7.42	2.86	15.8	19.4	39.4	40.7	16.4
Sr	101	168	39.2	182	179	79.7	79.1	197	95.6	547
Y	1.36	0.880	1.54	1.02	0.500	3.03	21.5	16.3	16.7	17.7
Zr	3.10	2.45	7.39	3.94	2.34	7.09	260	42.3	48.1	64.9
Nb	< 0.5	< 0.5	< 0.5	< 0.5	< 0.5	0.620	3.80	1.88	2.42	7.22
Hf	0.091	0.110	0.099	0.068	0.034	0.240	6.73	1.26	1.54	1.67
Ta	< 0.1	< 0.1	< 0.1	< 0.1	< 0.1	< 0.1	0.400	< 0.1	0.150	0.410
Th	< 0.1	< 0.1	0.360	< 0.1	0.150	0.260	1.38	0.140	0.170	1.54
U	< 0.1	< 0.1	< 0.1	< 0.1	< 0.1	< 0.1	0.320	< 0.1	< 0.1	0.240
Cu	50.7	70.9	59.5	91.8	33.4	100	91.3	97.3	144	158
Zn	75.7	62.6	44.1	82.0	38.5	109	68.3	129	148	296
La	0.470	0.500	6.78	0.610	4.53	1.17	3.26	8.45	7.25	25.8
Ce	0.980	1.35	7.06	1.11	5.16	3.57	5.84	19.5	17.0	55.0
Pr	0.120	0.130	0.570	0.160	0.400	0.450	0.720	2.68	2.17	6.78
Nd	0.760	0.750	1.96	0.790	1.04	1.66	3.06	11.2	9.33	29.4
Sm	0.160	0.130	0.330	0.270	0.240	0.440	1.28	2.88	1.99	5.96
Eu	0.089	0.210	0.360	0.140	0.140	0.280	0.270	1.13	0.890	3.37
Gd	0.150	0.240	0.340	0.190	0.180	0.470	1.79	2.91	2.63	8.66
Tb	0.028	0.025	0.056	0.024	0.024	0.083	0.390	0.420	0.360	0.650
Dy	0.230	0.180	0.270	0.200	0.130	0.490	2.91	2.57	2.70	3.21
Ho	0.048	0.036	0.066	0.031	0.019	0.110	0.810	0.600	0.640	0.710
Er	0.120	0.088	0.150	0.120	0.048	0.290	2.49	1.90	1.97	1.82
Yb	0.130	0.120	0.110	0.092	0.044	0.350	2.37	1.60	1.85	1.36
Lu	0.017	0.019	0.012	0.012	0.005	0.057	0.400	0.290	0.290	0.210

Note. Sample 2202 is protolith for garnetites 2204 and 2208.

The amount of Y in two garnetites after peridotites (samples 2208 and 2204) is low and similar to that of their protolith (0.50 and 1.54 ppm). Y in garnetite (sample 2226) increases abruptly up to 21.5 ppm relative to the protolith (3.03 ppm). In garnetite after porphyrite (sample 2234), Y remains unchanged (17.7 ppm) upon transition from the original rock.

The behavior of Zr correlates with that of Y. The amount of Zr in samples 2208 and 2204 (2.34 and 7.39 ppm) is consistent with that of the protolith. The amount of Zr in garnetite (sample 2226) increases abruptly relative to that in the protolith (260 and 7.09 ppm, respectively). In garnetite after porphyrite (sample 2234) Zr increases to 64.9 ppm (from 42.3 ppm in the protolith).

Niobium behaves like zirconium, reaching a maximum concentration of 7.22 ppm in garnetite after porphyrite (sample 2234). A similar trend is displayed by other HFSE: hafnium (maximum concentration in sample 2226 is 6.73 ppm); tantalum (only in garnetites from samples 2226 and 2234 its concentration of about 0.4 ppm is above the detection limit); thorium (it reaches a maximum concentration of about 0.4 ppm in garnetites from samples 2226 and 2234) and uranium (its distribution is similar to that of tantalum).

Rare earth elements. A common trend for garnetites is the growth of total REE concentration relative to that of their protoliths. REE concentration for samples 2208 and 2204 is 12.0 and 18.1 ppm, as compared with 3.34 ppm in the protolith (peridotite). REE concentration increases from 9.47 to 26.0 ppm for samples 2223 (garnetiferous peridotite) and 2226 (garnetite). The greatest increase in REE is displayed by garnetite after porphyrite (sample 2234) – from 56.4 ppm in porphyrite to

This is an open access article under the CC BY 4.0 license

Journal of Mining Institute. 2023. Vol. 262. P. 509-525
© Laysan I. Salimgaraeva, Alexei V. Berezin, 2023

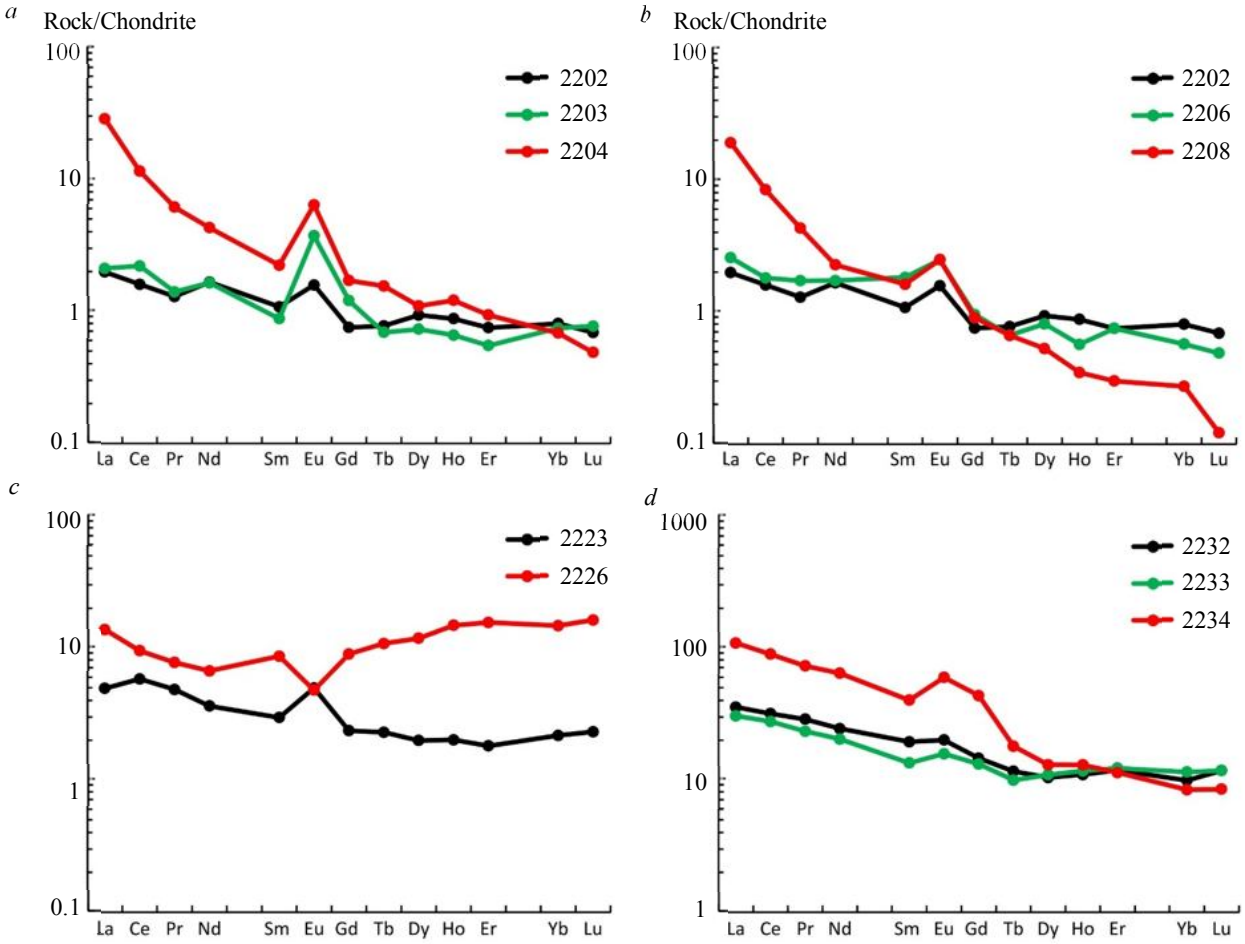


Fig.4. REE distribution spectra in the studied rocks: 2202, 2223 – ultrabasites; 2232 – porphyrite; 2203, 2206, 2233 – eclogites; 2204, 2208, 2226, 2234 – garnetites

143 ppm in garnetite. For samples 2204 and 2208, REE increases mainly due to the increased amount of LREE. In garnetite after porphyrite, LREE increase along with medium and some HREE.

The above REE distribution pattern is clearly displayed by spectra for garnetites, as compared with those for their protoliths (Fig.4). The protoliths, such as peridotite (sample 2202) and eclogite, which evolves after it (sample 2203), are similar in REE distribution and concentration (Fig.4, *a*), except Eu and partly Gd, which increase in eclogite. However, garnetite (sample 2204) contains elevated concentrations of all light (growth is most substantial) and medium REE, heavy REE also increase (except Yb and Lu), but not so markedly. The REE fractionation index (La_N/Lu_N ratio) for garnetite increases to 58.7 (from 2.87 and 2.73 in peridotite and eclogite). All three samples in this series exhibit a positive Eu-anomaly, which is comparable for eclogite and garnetite (Eu/Eu* = 3.62 and 3.28, respectively); Eu/Eu* for peridotite is 1.75.

There are some differences in the rock series consisting of peridotite (sample 2202), eclogite (sample 2206) and garnetite (sample 2208), because only light REE are accumulated in garnetite (Fig.4, *b*). As HREE are removed, garnetite displays maximum REE fractionation (La_N/Lu_N = 157), as compared with peridotite and eclogite (2.87 and 5.28, respectively). Eu-anomaly for the rocks of this series is positive (Eu/Eu* = 1.75-2.05).

Peridotite (sample 2223) and garnetite (sample 2226) differ in a REE distribution pattern from other rocks (Fig.4, *c*). The REE spectrum for peridotite is complementary to that for other peridotite (sample 2202), while the REE spectrum for garnetite shows a slightly differentiated pattern. Curiously, Eu concentration remains practically unchanged upon transition from peridotite to garnetite, the sign of Eu-anomaly changes from positive to negative, but its amplitude remains unchanged. REE

This is an open access article under the CC BY 4.0 license

distribution in garnetite attains some features of a "bird's wings" spectrum characteristic of rocks, which have experienced strong fluid reworking [42].

The REE distribution spectra of porphyrite (sample 2232) and eclogite (sample 2233) are similar (Fig.4, *d*). Garnetite differs from them in elevated amounts of light and medium REE and Gd. The degree of REE fractionation (La_N/Lu_N = 12.8) is not so high as that for samples 2204 and 2208, increasing relative to that of porphyrite and eclogite (3.02 and 2.59, respectively). Eu-anomaly for three samples is moderate and positive (Eu/Eu* = 1.19 for porphyrite and eclogite and 1.43 for garnetite).

Major element composition of minerals. *Garnetites evolving after peridotites.* In sample 2204, garnets occur as solid rocks with scarce amphibole (pargasite) grains up to 300 μm across (Fig.5, *a*). The garnets are heterogeneous in composition: mol.% is 48-59 for Prp, 21-27 for Alm, 14-26 for Grs and no more than 1.2 for Sps (Table 3). One regularity is note-worthy: at the contact with an amphibole zone, Grs content increases (14-17 mol.%), as does Prp content (55-59 mol.%) relative to the portion of the sample far away from the contact, where Grs makes up 24-27 mol.% and Prp is 43-49 mol.% (Table 3). Alm content in different zones remains practically unchanged. The Mg content of garnets at the contact with an amphibole zone is 0.65-0.70 and away from the zone 0.61-0.66; the Mg content of amphiboles is invariable: 0.87-0.88 (Table 4). Analysis of #Mg in garnets and amphiboles indicates no equilibrium between the two minerals and the relatively rapid evolution of the garnetite zone.

In sample 2208, garnets are present as idiomorphic grains measuring from 250 to 500 μm in the matrix (Fig.5, *b*), which consists mainly of amphiboles (pargasite) and epidote-group minerals (zoisite). The garnets have no inclusions and display no major-element zoning. However, Prp makes up 48-52 mol.%, Alm content is less than 17-23 mol.%, and Grs is greater than 26-31 (see Table 3), as compared to sample 2204.

Table 3

Representative analyzes of the composition of garnets by major elements, wt.%

Mineral	2204						2208			2226		
	7	8	10	15	17	21	3	4	23	4	12	13
SiO_2	40.98	41.59	41.65	39.90	40.69	41.09	41.23	40.92	41.12	40.89	40.83	40.38
Al_2O_3	22.72	22.66	22.72	22.40	22.62	22.93	23.42	22.88	22.98	22.46	22.29	22.60
Fe_2O_3t	13.98	14.17	12.60	15.14	13.36	12.22	10.14	10.08	10.22	16.25	16.75	16.47
MnO	0.45	0.37	0.48	0.61	0.42	0.49	0.19	0.18	0.19	0.81	0.47	0.74
MgO	15.36	15.26	16.43	11.72	13.34	13.58	13.61	14.03	13.67	13.02	13.23	13.89
CaO	6.50	5.94	6.12	10.23	9.57	9.70	11.41	11.91	11.82	6.58	6.43	5.92
Total	99.99	99.99	100.0	100.0	100.0	100.0	100.0	100.0	100.0	100.0	100.0	100.0
Prp	55.87	55.11	58.83	43.78	48.88	49.28	49.30	51.11	49.57	47.63	48.30	51.28
Alm	26.20	28.70	24.46	27.45	25.06	24.43	20.61	17.33	19.25	33.37	33.86	31.46
Grs	17.00	15.43	15.74	27.48	25.19	25.29	29.69	31.19	30.78	17.31	16.88	15.72
Sps	0.94	0.76	0.96	1.28	0.87	1.00	0.40	0.37	0.40	1.69	0.96	1.54

Mineral	2234				2224				2225			
	21	22	23	24	2*c*	3*r*	18*c*	19*r*	40*c*	38*r*	44*c*	55*r*
SiO_2	38.18	38.10	38.13	38.05	39.87	40.30	39.85	39.83	39.45	39.23	39.35	39.02
Al_2O_3	20.81	21.10	20.99	21.27	22.54	22.43	22.46	22.09	21.83	21.16	21.78	22.11
Fe_2O_3t	26.86	27.00	26.59	26.84	16.64	17.07	16.98	17.59	20.54	21.55	19.82	21.42
MnO	0.59	0.62	0.65	0.43	0.44	0.19	0.15	0.48	0.29	0.11	0.43	0.37
MgO	3.73	3.67	3.48	3.87	10.67	11.24	9.81	11.08	8.49	9.12	7.83	9.48
CaO	9.83	9.52	10.15	9.54	9.84	8.77	10.00	8.35	10.13	7.53	10.80	7.61
Total	100.0	100.0	99.99	100.0	100.0	100.0	99.25	99.42	100.7	98.70	100.0	100.0
Prp	14.56	14.36	13.61	15.17	39.89	41.58	36.86	41.46	32.08	34.65	29.67	36.22
Alm	56.55	57.50	56.44	57.01	32.73	34.72	35.79	35.05	39.78	44.55	39.99	42.07
Grs	27.59	26.78	28.52	26.85	26.44	23.30	27.01	22.45	27.51	20.57	29.40	20.90
Sps	1.30	1.37	1.43	0.97	0.94	0.40	0.33	1.04	0.64	0.23	0.94	0.81

Note. Numbers of samples and numbers of points of analysis are indicated; *c* – core of grain, *r* – rim.

This is an open access article under the CC BY 4.0 license

Journal of Mining Institute. 2023. Vol. 262. P. 509-525
© Laysan I. Salimgaraeva, Alexei V. Berezin, 2023

Table 4

Representative analyzes of the composition of rock-forming minerals by major elements, wt.%

Mineral	Amphiboles			Clinopyroxenes		Epidote group minerals		
	2204	2208	2226	2226	2225	2208	2225	2234
SiO_2	45.32	45.30	46.94	54.24	54.35	40.04	38.50	36.05
TiO_2	0.40	0.19	0.45	0.07	0.08	–	0.19	–
Al_2O_3	15.74	17.29	12.54	0.80	9.35	33.66	29.23	25.82
Fe_2O_3t	4.39	2.76	5.35	2.76	4.71	0.57	5.32	8.53
MnO	0.03	0.00	0.11	0.17	–	0.02	–	–
MgO	17.48	17.09	17.66	16.26	9.68	0.11	0.32	0.00
CaO	13.75	13.06	13.71	25.79	17.25	26.42	25.01	22.89
Na_2O	2.67	2.90	2.35	0.27	5.03	–	–	–
K_2O	0.40	0.09	0.14	–	–	–	–	–
Cl	0.10	–	–	–	–	–	–	–
Total	100.28	98.68	99.25	100.36	100.45	100.82	98.57	93.65
Element	Crystallochemical coefficients							
Si	6.276	6.278	6.569	1.977	1.952	2.969	2.995	3.012
Ti	0.042	0.020	0.047	0.002	0.002	–	0.011	–
Al	2.569	2.824	2.068	0.034	0.396	2.942	2.680	2.543
Fe	0.508	0.320	0.626	0.084	0.141	0.035	0.346	0.596
Mn	0.004	–	0.013	0.005	–	0.001	–	–
Mg	3.608	3.531	3.685	0.884	0.518	0.012	0.037	–
Ca	2.040	1.939	2.056	1.007	0.664	2.099	2.085	2.049
Na	0.717	0.779	0.638	0.019	0.350	–	–	–
K	0.071	0.016	0.025	–	–	–	–	–
Cl	0.023	–	–	–	–	–	–	–

Sample 2226 displays lenticular aggregates of xenomorphic garnets in the matrix composed of hypidiomorphic clinopyroxene (diopside) grains up to 300 μm across (Fig.5, *c*). Furthermore, single amphibole (pargasite), ilmenite and Cl-apatite grains are occasionally encountered. The major-element composition of the garnets varies slightly. It is similar in Prp content (47-51 mol.%) to the composition of garnets from samples 2204 and 2208. However, garnets from sample 2206 contain low Grs (15-19 mol.%) and elevated Alm (30-33 mol.%) content.

Garnets in samples 2224 and 2225 occur as coarse well-faceted porphyroblasts measuring up to 500 μm with scarce quartz inclusions (Fig.5, *d*, *e*). The matrix is dominated by quartz; scarce xenomorphic omphacite (Na_2O content is up to 5 wt.%) and epidote grains occur. Rutile and Cl-apatite are present as accessories. Garnets from sample 2224 contain more magnesium (#Mg = 0.50-0.57) than those from sample 2225 (#Mg = 0.38-0.46). Grs and

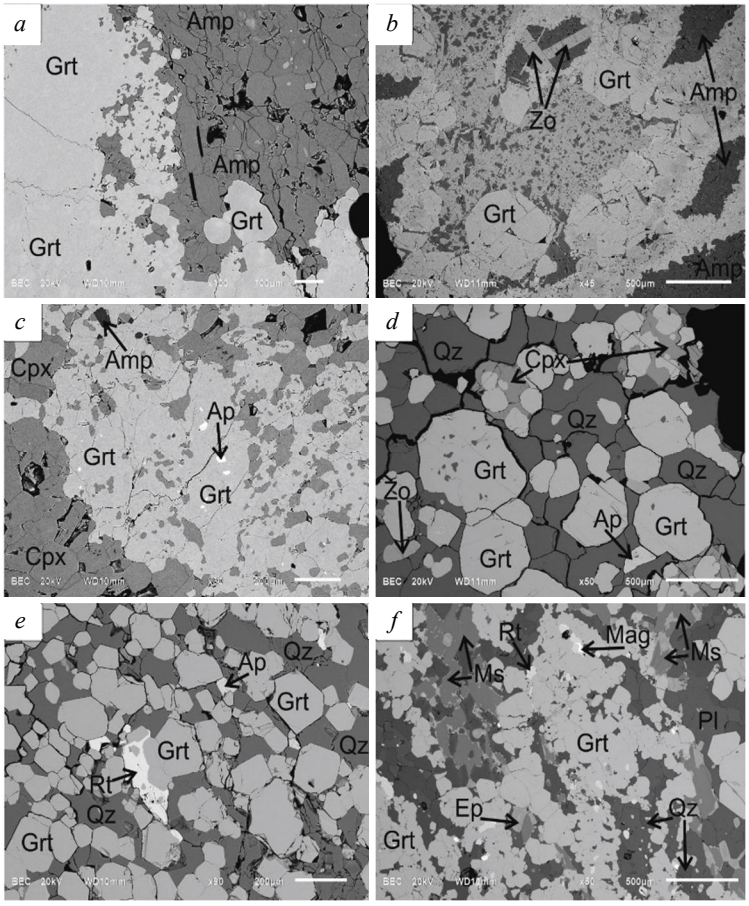


Fig.5. BSE-images of garnetites associated with peridotites: sample 2204 (*a*); sample 2208 (*b*); sample 2226 (*c*); sample 2225 (*d*); sample 2224 (*e*); with porphyrites: sample 2232 (*f*)

This is an open access article under the CC BY 4.0 license

Sps contents in the above samples are similar: Grs – 20-29 mol.%, Sps – 0.2-1.1 mol.%. The garnets display poorly-defined zoning with an increase in Prp and Alm (by 3-5 mol.%) and a decrease in Grs content (by 3-9 mol.%) from the centre to the margin of grains (see Table 3).

Garnetites evolving after basic porphyrites. In garnetites (sample 2234), garnets are present as aggregates of "agglutinated" porphyroblasts measuring 50 to 400 μm (Fig.5, *f*). Space between garnet aggregates is filled mainly with plagioclase (An_{9-10}), quartz, epidote and muscovite grains. Accessory mineral (rutile and magnetite) grains occur. All garnets from this sample, including fine grains with indiscernible boundaries, contain the following end-members content, mol.%: Alm – 55-61; Prp – 9-16; Grs – 24-29; Sps – 0.8-1.4 (see Table 3).

Thus, the composition of garnets from garnetites is largely controlled by the composition of the protolith after which they evolve (Fig.6).

Trace element composition of minerals. Garnets from sample 2208 contain minimum HFSE concentrations, as compared to other garnetites, ppm: Y – 0.7; Ti – 58.3 on the average; Hf – no more than 0.1 and V – 72.0 on the average (Table 5).

In garnets from other garnetites (samples 2224-2226, 2204 and 2234), Y is as high as 14.5-147 ppm (average value is is 44.4 ppm). Ti varies 109-381 ppm (240 ppm on the average), Hf is 0.43-7.56 ppm (2.29 ppm on the average). Elevated Cr concentrations (637 ppm on the average) are present in garnet from sample 2204 and elevated V concentrations in garnet from sample 2224 (average value is 201 ppm).

Garnets from garnetite after porphyrite (sample 2234) contain elevated Ti (average value is 356 ppm) and lowered V and Cr (average values are 49.6 and 57.7 ppm, respectively). Garnets from this sample exhibit the zonal distribution of some trace elements. The central portion of a grain is enriched in HFSE (Ti, Zr and Hf) and depleted in V and Cr relative to the rim (Table 5).

Rare earth elements. Garnets from sample 2208 contain minimum REE concentrations (ΣREE ~0.49 ppm). REE distribution spectra for garnets from sample 2208 (Fig.7, *a*) display the same differentiated pattern for other garnets in the light REE domain, but in medium and heavy REE domains the spectra are highly flattened (Lu_N/Gd_N ~1.40). Garnets from sample 2208 show a positive Eu-anomaly. Its amplitude decreases slightly from the core to the rim of a grain (Eu/Eu* = 4.22 and 2.48, respectively). This pattern of the spectra, not typical of metamorphic garnets, could be due to inheritance from a precursor mineral, presumably plagioclase [42].

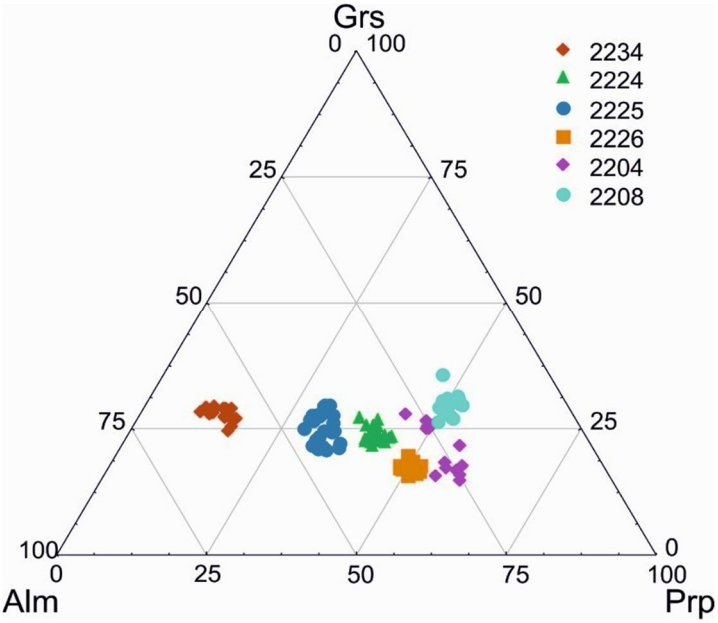


Fig.6. Diagram of Prp-Grs-Alm content in garnets from garnetites

REE distribution spectra in garnets from other garnetites display a differentiated distribution pattern with an increase in normalized concentration from light to heavy REE. A common feature for garnets from samples 2224-2226 and 2234 is the flattening of part of their spectrum in the heavy REE domain (Lu_N/Gd_N ~2.75). For garnet from sample 2204, heavy REE are differentiated in the same manner as light REE (Lu_N/Gd_N ~13.30). Garnets from samples 2224-2226 display a moderate negative Eu-anomaly (Eu/Eu* 0.54-0.96). Garnets from garnetite after porphyrite (sample 2234) show a positive Eu-anomaly (Eu/Eu* ~2.13).

This is an open access article under the CC BY 4.0 license

Journal of Mining Institute. 2023. Vol. 262. P. 509-525
© Laysan I. Salimgaraeva, Alexei V. Berezin, 2023

Table 5

Representative analyzes of the composition of rock-forming minerals by trace elements, ppm

Mineral	Garnets												
	2226			2204		2208			2234			2224	
	3*r*	4*m*	5*c*	9	10	11*r*	12*c*	13*r*	20*r*	21*c*	22*r*	25*r*	26*c*
La	0.012	0.039	0.087	0.011	0.011	*bdl*	0.007	*bdl*	0.018	0.009	0.009	0.005	*bdl*
Ce	0.083	0.084	0.128	0.016	0.011	0.014	0.007	0.017	0.050	0.043	0.029	0.027	0.017
Pr	0.031	0.047	0.039	*bdl*	0.005	*bdl*	*bdl*	*bdl*	0.009	0.007	0.011	0.005	0.004
Nd	0.749	0.832	0.722	0.070	0.043	*bdl*	*bdl*	*bdl*	0.143	0.248	0.059	0.036	0.056
Sm	1.58	1.24	1.63	0.147	0.177	0.050	0.038	0.039	0.666	0.693	0.247	0.047	0.149
Eu	0.550	0.492	0.667	0.075	0.082	0.067	0.080	0.030	1.00	1.19	0.418	0.028	0.115
Gd	4.38	4.37	4.94	0.381	0.447	0.074	0.088	0.086	2.96	3.38	1.94	0.237	1.61
Tb	1.03	0.947	1.11	0.114	0.123	0.012	0.027	0.017	0.737	0.769	0.564	0.232	0.487
Dy	7.06	5.47	6.48	1.36	1.78	0.137	0.137	0.076	5.08	5.02	3.77	2.84	4.28
Er	4.12	2.40	2.99	2.52	2.80	0.058	0.081	0.074	2.72	2.19	2.09	3.33	4.25
Yb	3.43	1.71	2.12	4.54	4.01	0.028	0.065	0.080	2.16	1.243	1.30	3.62	4.98
Lu	0.463	0.344	0.411	0.739	0.604	0.012	0.017	0.013	0.326	0.308	0.207	0.448	0.661
Ti	237	208	217	109	112	57.1	64.4	53.4	332	381	355	266	214
V	123	123	128	100	110	70.4	67.9	77.8	43.5	32.7	72.5	192	210
Cr	202	149	213	670	604	296	305	309	61.7	50.1	61.2	190	170
Y	43.9	29.1	36.3	14.5	17.5	0.682	0.717	0.651	31.8	27.2	25.1	26.5	34.8
Zr	16.7	11.4	16.1	8.41	8.25	2.24	2.56	2.03	5.66	8.29	5.84	9.04	2.15
Ba	0.226	0.146	0.464	0.191	0.187	0.237	0.231	0.195	0.666	0.372	0.332	0.575	0.403
Hf	2.29	2.10	2.32	0.430	0.571	0.099	0.083	0.102	1.76	2.22	1.40	1.01	1.22

Mineral	Garnets			Amphiboles			Clinopyroxenes		Epidote		Zoisite	Muscovite
	2225			2226	2204	2208	2226	2225	2225	2234	2208	2234
	30*r*	31*c*	32*r*	6	7	14	1	28	29	18	15	19
La	0.051	0.015	0.052	8.70	2.05	0.867	1.63	0.032	1219	1795	38.2	4.62
Ce	0.088	0.060	0.080	24.7	5.44	0.861	4.62	0.180	2422	3750	43.0	0.10
Pr	0.020	0.009	0.015	3.72	0.766	0.075	0.644	0.023	305	472	4.06	0.008
Nd	0.211	0.093	0.152	23.8	4.52	0.392	3.53	0.148	1374	2311	16.3	0.097
Sm	0.597	0.251	0.343	8.06	0.718	0.056	1.36	0.088	238	439	2.42	0.210
Eu	0.317	0.172	0.285	1.49	0.327	0.023	0.196	0.038	26.9	208	2.24	*bdl*
Gd	5.33	3.24	4.57	7.51	1.39	0.081	0.748	0.377	138	261	0.862	*bdl*
Tb	1.46	1.44	2.36	0.755	0.081	0.016	0.075	0.093	7.97	8.19	0.078	0.008
Dy	7.58	12.5	21.3	3.23	0.657	0.038	0.454	0.433	62.7	55.0	0.436	0.814
Er	4.99	11.0	14.7	0.673	0.288	0.066	0.113	0.123	13.0	13.8	0.086	0.233
Yb	5.33	9.36	11.1	0.338	0.077	0.022	0.096	0.188	7.45	2.08	0.121	0.086
Lu	0.854	1.23	1.45	0.153	0.035	*bdl*	0.022	0.009	2.57	2.59	0.008	0.030
Ti	198	246	246	2769	2251	667	369	1342	1148	828	84.8	8762
V	122	126	109	329	163	97.8	56.4	549	522	167	15.7	573
Cr	404	288	261	668	833	554	275	546	687	59.7	256	54.0
Y	53.4	89.3	147	8.47	2.34	0.347	1.22	1.70	165	66.5	2.21	0.882
Zr	3.54	2.60	3.81	19.6	12.8	1.67	1.81	10.8	18.2	17.8	1.16	2.00
Ba	1.62	1.26	1.41	120	96.1	76.3	0.107	0.862	18.1	44.9	17.3	6276
Hf	2.38	4.56	7.56	2.18	0.618	0.119	0.281	0.759	13.6	6.89	0.121	1.34

Notes: *c* – core of grain; *m* – medium; *r* – rim; *bdl* – below detection limit.

Amphiboles from samples 2226, 2204, and 2208 are markedly different in a REE distribution pattern (Fig.7, *b*). Average total REE is 1.37 ppm for sample 2208, 83.4 ppm for sample 2206, and 15.5 ppm for sample 2204. Ti concentration varies in a similar manner: 697, 2769 and 2258 ppm, respectively. Anomalously low REE concentration in amphibole seems to indicate the metasomatic genesis of the mineral [43]. REE distribution spectra in amphiboles from samples 2226 and 2204 are conformal between each other, differing only in total REE concentration. They display a convex spectrum in light and medium REE domains. Two spectra for amphibole from sample 2208 exhibit an extremely low light REE concentration level, coinciding roughly in medium and heavy REE domains (Fig.7, *b*).

This is an open access article under the CC BY 4.0 license

© Laysan I. Salimgaraeva, Alexei V. Berezin, 2023

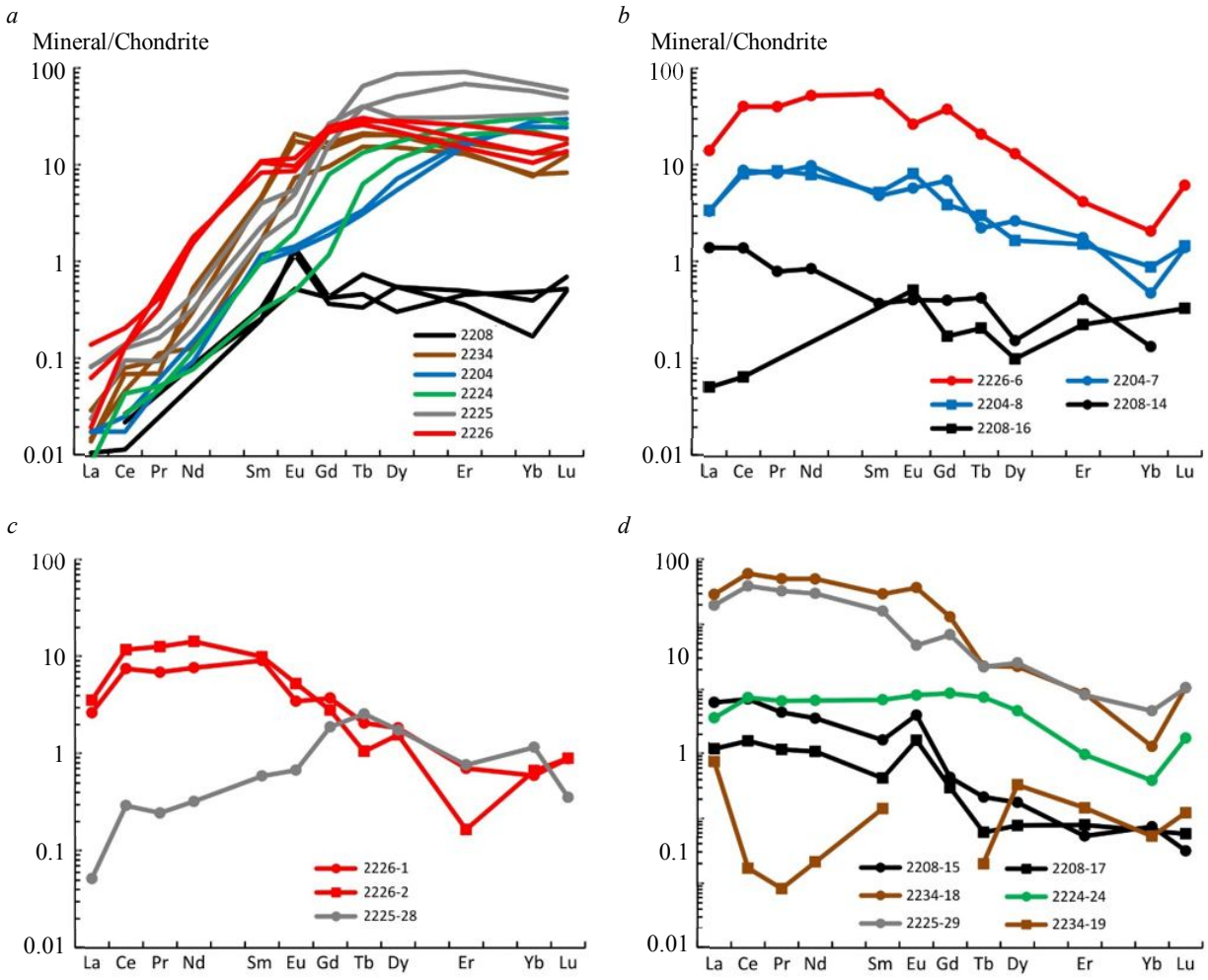


Fig.7. REE distribution spectra in the rock-forming minerals from garnetites: garnet (*a*); amphiboles (*b*); pyroxenes (*c*); epidote group minerals (*d*)

REE distribution spectra in pyroxenes from sample 2226 imitate the configuration of the spectrum for amphiboles from the same sample (Fig.7, *c*). The REE spectrum for pyroxenes from sample 2225 display lowered light REE concentration and a more differentiated distribution pattern in the LREE domain. In the heavy REE domain, spectra for all three analyzed pyroxenes are similar to each other.

Total REE concentrations in epidote from samples 2225 and 2234 are 5819 and 9318 ppm, respectively. Their distribution spectra are highly differentiated (Fig.7, *d*). Epidote from sample 2224 shows more moderate REE concentration (154 ppm) and a horizontal spectrum in light and medium REE domains. Zoisite from sample 2208 displays a low light REE concentration level (108 and 25.6 ppm). Its REE distribution spectra are similar to those for epidote from samples 2225 and 2234. One difference is a well-defined positive Eu-anomaly in sample 2208 (Eu/Eu* ~4.65). Sr and Ba concentrations in epidote and zoisite from different samples are comparable (Sr ~3930 ppm in epidote and 4911 ppm in zoisite; Ba ~24.5 ppm in epidote and 18.2 ppm in zoisite).

Muscovite was analyzed only from sample 2234. Its REE concentration is as low as that of chondrite, except La (over 10 chondrite ratios, Fig.7, *d*).

Conclusions. It follows from the petrographic characteristics of the rocks studied that the primary magmatic association experienced two stages of metamorphism. At stage I (autometamorphism), serpentine, chlorite and garnet were formed in ulrabasic rocks. At stage II, garnetites and eclogites were formed, and zoisite and muscovite emerged.

This is an open access article under the CC BY 4.0 license

Journal of Mining Institute. 2023. Vol. 262. P. 509-525
© Laysan I. Salimgaraeva, Alexei V. Berezin, 2023

Field work and petrographic studies showed that the rocks were metamorphosed at 550-600 °C (the presence of epidote in granites and chlorite in ultrabasic and basic rocks). Felsic (host) rocks were migmatized at this temperature, and part of melt could migrate [22, 44]. In this case, basic and ultrabasic rocks practically remain rigid and display mainly brittle deformations, as shown by field studies above veined garnetites in ultrabasic rocks. Host rocks are slightly migmatized and reworked. Features of the manifestation of garnetization processes in rocks with the appearance of confluent, up to monomineral, aggregates, without the formation of well-faceted crystals, indicate that it proceeded subsynchronously with the appearance of eclogites, was rather short-lived and had a nuclear character. The formation of garnetitic aggregates in intergranular space indicates that fluid contributed actively to their formation.

It is hard to imagine that genetically different rocks with similar mineral associations (eclogites and granitites) were tectonically combined in such a limited area as Slyudyanaya Gorka. The occurrence of ultrabasic and basic rock and sublvolcanic rock blocks with garnetites and eclogites evolving after them suggests that granitites formed simultaneously after protoliths of all types.

A probabilistic model for the formation of an eclogite-garnetite association is tentatively presented as the following sequence.

The penetration of a fluid enriched in Na, Al, and possibly water along fractures in the protolith provokes the formation of metasomatic column by diffusion. The column includes zones enriched in garnet and Na-pyroxene (up to omphacite). This sequence is consistent with the authors' mass-balance estimates indicative of Na and Ti mobility. Previously, it was shown that Ti and Zr could migrate in metasomatic fluid together with U, Th, Y and REE [45]. A triple increase in La and Ce in garnetites relative to their protolith cannot be interpreted from the standpoint of isochemical metamorphism. However, the above elements are isomorphically included in the minerals of epidote group, with which the host granitoids are often saturated. Correspondingly, these elements would pass into fluid even upon slight migmatization. The fluid formed in the rocks is highly alkaline, which contributes to the successful migration of the above elements.

The above characteristics show that the model for the mantle genesis of Marun-Keu eclogites and granitites may not be fully applicable, as some authors argued [46]. For example, the presence of eclogitized anorthosite blocks either in oceanic crust sequences or in the lower portion of the continental crust [47], or eclogitized and garnetized basic porphyrites, the textural and structural characteristics of which clearly indicate the shallow depths of formations. Therefore, one of probable models for the formation of Marun-Keu eclogites and garnetites is the eclogitization of the oceanic crust followed by its uplifting to upper levels. Such a possibility has been put forward earlier [17]. The classical section of the oceanic crust (ultrabasic rocks with chromite, cumulative rocks, and subvolcanic bodies) and the distinctive characteristics of Slyudyanaya Gorka rocks are consistent with this option. The formation of these rocks in the lower continental crust is less probable, because no granulite associations have been found.

Slyudyanaya Gorka granitites seem to have been derived from basic and ultrabasic crustal rocks during their uplifting to higher levels of the section affected by the crustal fluid penetrating along fracturing zones.

The authors are grateful to S.G.Simakin, E.V.Potapov (Valiev IPT RAS, Yaroslavl branch), O.L.Galankina (IPGG RAS) for their help in analytical studies.

REFERENCES

1. Gottman I.A., Pushkarev E.V., Khiller V.V. Uranium-bearing srilankite from high-pressure garnetites in the Southern Urals – first data. *Doklady Akademii nauk*. 2018. Vol. 479. N 6, p. 677-681 (in Russian). DOI: 10.7868/S0869565218120150

2. Selyatitskii A.Yu., Reverdatto V.V. Thermobaric Conditions for Exhumation of Ti-Clinohumite Garnetites of the Kokchetav Subduction-Collision Zone (Northern Kazakhstan). *Russian Geology and Geophysics*. 2022. Vol. 63. N 8, p. 1051-1074. DOI: 10.15372/GiG2021147

This is an open access article under the CC BY 4.0 license

3. Yung-Hsin Liu, Huai-Jen Yang, Yen-Hong Shau et al. Compositions of high Fe-Ti eclogites from the Sulu UHP metamorphic terrane, China: HFSE decoupling and protolith characteristics. *Chemical Geology*. 2007. Vol. 239. Iss. 1-2, p. 64-82. DOI: 10.1016/j.chemgeo.2006.12.005

4. Irifune T., Sekine T., Ringwood A.E., Hibberson W.O. The eclogite-garnetite transformation at high pressure and some geophysical implications. *Earth and Planetary Science Letters*. 1986. Vol. 77. Iss. 2, p. 245-256. DOI: 10.1016/0012-821X(86)90165-2

5. Nishi M., Kubo T., Kato T. Metastable transformations of eclogite to garnetite in subducting oceanic crust. *Journal of Mineralogical and Petrological Sciences*. 2009. Vol. 104. Iss. 3, p. 192-198. DOI: 10.2465/jmps.080929

6. Sekine T., Irifune T., Ringwood A.E., Hibberson W.O. High-pressure transformation of eclogite to garnetite in subducted oceanic crust. *Nature*. 1986. Vol. 319. Iss. 6054, p. 584-586. DOI: 10.1038/319584a0

7. Bakker R.J., Pushkarev E., Biryuzova A.P. High Temperature Reduced Granulite-Facies Nature of Garnetites in the Khabarny Mafic–Ultramafic Massif, Southern Urals: Evidence from Fluid and Mineral Analyses. *Journal of Petrology*. 2020. Vol. 61. Iss. 6, p. 1-25. DOI: 10.1093/petrology/egaa066

8. Shujuan Jiao, Jinghui Guo, Harley S.L., Windley B.F. New Constraints from Garnetite on the P-T Path of the Khondalite Belt: Implications for the Tectonic Evolution of the North China Craton. *Journal of Petrology*. 2013. Vol. 54. Iss. 9, p. 1725-1758. DOI: 10.1093/petrology/egt029

9. Schwandt C.S., Papike J.J., Shearer C.K., Brearley A.J. A Sim investigation of REE chemistry of garnet in garnetite associated with the Broken Hill Pb-Zn-Ag orebodies, Australia. *The Canadian Mineralogist*. 1993. Vol. 31. N 2, p. 371-379. DOI: 10.3749/1499-1276-31.2.371

10. Spry P.G., Heimann A., Messerly J.D., Houk R.S. Discrimination of Metamorphic and Metasomatic Processes at the Broken Hill Pb-Zn-Ag Deposit, Australia: Rare Earth Element Signatures of Garnet-Rich Rocks. *Economic Geology*. 2007. Vol. 102. Iss. 3, p. 471-494. DOI: 10.2113/gsecongeo.102.3.471

11. Early Precambrian of the Baltic Shield. Edited by V.A.Glebovitsky. St. Petersburg: Nauka, 2005, p. 711 (in Russian).

12. Vrijmoed J.C., Austrheim H., John T., Podladchikov Y.Y. Metasomatism of the UHP Svartberget olivine-websterite body in the Western Gneiss Complex, Norway. *Geochimica et Cosmochimica Acta Supplement*. 2008. Vol. 72. N 12, p. A989.

13. Kropáč K., Buriánek D., Zimák J. Origin and metamorphic evolution of Fe-Mn-rich garnetites (coticules) in the Desná Unit (Silesicum, NE Bohemian Massif). *Geochemistry*. 2012. Vol. 72. Iss. 3, p. 219-236. DOI: 10.1016/j.chemer.2011.11.002

14. Cruz-Uribe A.M., Page F.Z., Lozier E. et al. Trace element and isotopic zoning of garnetite veins in amphibolitized eclogite, Franciscan Complex, California, USA. *Contributions to Mineralogy and Petrology*. 2021. Vol. 176. Iss. 5. N 41. DOI: 10.1007/s00410-021-01795-4

15. van Schrojenstein Lantman H.W., Scambelluri M., Gilio M. et al. Extensive fluid-rock interaction and pressure solution in a UHP fluid pathway recorded by garnetite, Lago di Cignana, Western Alps. *Journal of Metamorphic Geology*. 2021. Vol. 39. Iss. 4, p. 501-518. DOI: 10.1111/jmg.12585

16. Melnik A.E., Berezin A.V., Skublov S.G. Age (U-Pb, Sm-Nd) and Geochemical Features of Garnetites in Salma Eclogites, the Belomorian Mobile Belt. *Proceedings of the Russian Mineralogical Society*. 2014. N 6, p. 17-33 (in Russian).

17. Liu Y.Y., Perchuk A.L., Ariskin A.A. High pressure metamorphism in the peridotitic cumulate of the Marun-Keu complex, Polar Urals. *Petrology*. 2019. Vol. 27. N 2, p. 138-160 (in Russian). DOI: 10.31857/S0869-5903272138-160

18. Selyatitskii A.Yu., Kulikova K.V. The first data on the occurence of UHP metamorphism in the Polar Urals. *Doklady Akademii nauk*. 2017. Vol. 476. N 2, p. 1222-1225. DOI: 10.7868/S086956521730017X

19. Fancong Meng, Yazhou Fan, Shmelev V.R., Kulikova K.V. Constraints of eclogites from the Marun-Keu metamorphic complex on the tectonic history of the Polar Urals (Russia). *Journal of Asian Earth Sciences*. 2020. Vol. 187. N 104087. DOI: 10.1016/j.jseaes.2019.104087

20. Selyatitskii A.Yu., Kulikova K.V. Garnet as indicator of the protolith type of UHP-peridotites from Marun-Keu complex (Polar Urals, Russia). *Vestnik of Institute of Geology of Komi Science Center of Ural Branch RAS*. 2018. N 2, p. 38-47 (in Russian). DOI: 10.19110/2221-1381-2018-2-38-47

21. Selyatitskii A.Yu., Kulikova K.V. Chemical evolution of garnet during metamorphism of peridotites from UHP Marun-Keu complex, Polar Ural. *Vestnik of Institute of Geology of Komi Science Center of Ural Branch RAS*. 2017. N 8, p. 36-43 (in Russian). DOI: 10.19110/2221-1381-2017-8-36-43

22. Udovkina N.G. Eclogites of the Polar Urals (on the example of southern part of Marun-Keu ridge). Moscow: Nauka, 1971, p. 191 (in Russian).

23. Abdrakhmanov I.A., Gulbin Yu. L., Gembitskaya I.M. Fe-Mg-Al-Ti-Zn Oxide Assemblage in Granulites of the Bunger Hills, East Antarctica: Evidence of Ultrahigh-Temperature Metamorphism. *Proceedings of the Russian Mineralogical Society*. 2021. Vol. 150. N 4, p. 38-76 (in Russian). DOI: 10.31857/S086960552104002X

24. Akimova E.Yu., Skublov S.G. Distribution of rare-earth elements in rock-forming minerals of corundum-bearing rocks of the Khitoostrov deposit (North Karelia). *Vestnik of Saint Petersburg University. Earth Sciences*. 2021. Vol. 66. N 4, p. 686-705 (in Russian). DOI: 10.21638/spbu07.2021.403

25. Anczkiewicz R., Szczepański J., Mazur S. et al. Lu-Hf geochronology and trace element distribution in garnet: Implications for uplift and exhumation of ultra-high pressure granulites in the Sudetes, SW Poland. *Lithos*. 2007. Vol. 95. Iss. 3-4, p. 363-380. DOI: 10.1016/j.lithos.2006.09.001

26. Melnik A.E., Skublov S.G., Rubatto D. et al. Garnet and zircon geochronology of the Paleoproterozoic Kuru-Vaara eclogites, northern Belomorian Province, Fennoscandian Shield. *Precambrian Research*. 2021. Vol. 353. N 106014. DOI: 10.1016/j.precamres.2020.106014

27. Levashova E.V., Popov V.A., Levashov D.S., Rumyantseva N.A. Distribution of trace elements controlled by sector and growth zonings in zircon from a miaskite pegmatite of the Vishnegorsky massif, the Southern Urals. *Journal of Mining Institute*. 2022. Vol. 254, p. 136-148. DOI: 10.31897/PMI.2022.29

28. Rumyantseva N.A., Skublov S.G., Vanshtein B.G. Zircon from Gabbroids of the Shaka Ridge (South Atlantic): U-Pb Age, Oxygen Isotope Ratios and Trace Element Composition. *Proceedings of the Russian Mineralogical Society*. 2022. Vol. 151. N 1, p. 49-73 (in Russian). DOI: 10.31857/S0869605522010099

This is an open access article under the CC BY 4.0 license

29. Skublov S.G., Rumyantseva N.A., Vanshtein B.G. et al. Zircon xenocrysts from the Shaka Ridge record ancient continental crust: New U-Pb geochronological and oxygen isotopic data. *Journal of Earth Science*. 2022. Vol. 33. Iss. 1, p 5-16. DOI: 10.1007/s12583-021-1422-2

30. Xiao-Xiao Ling, Qiu-Li Li, Huyskens M.H. et al. Matrix effects and improved calibration procedures for SIMS titanite U-Pb dating. *Chemical Geology*. 2022. Vol. 593. N 120755. DOI: 10.1016/j.chemgeo.2022.120755

31. Gavrilchik A.K., Skublov S.G., Kotova E.L. Trace Element Composition of Beryl from the Sherlovaya Gora Deposit, South-Eastern Transbaikalia, Russia. *Proceedings of the Russian Mineralogical Society*. 2021. Vol. 150. N 2, p. 69-82 (in Russian). DOI: 10.31857/S0869605521020052

32. Abdel Gawad A.E., Ene A., Skublov S.G. et al. Trace Element Geochemistry and Genesis of Beryl from Wadi Nugrus, South Eastern Desert, Egypt. *Minerals*. 2022. Vol. 12. Iss. 2. N 206. DOI: 10.3390/min12020206

33. Skublov S.G., Gavrilchik A.K., Berezin A.V. Geochemistry of beryl varieties: comparative analysis and visualization of analytical data by principal component analysis (PCA) and t-distributed stochastic neighbor embedding (t-SNE). *Journal of Mining Institute*. 2022. Vol. 255, p. 455-469. DOI: 10.31897/PMI.2022.40

34. Sukhanova K.G., Kuznetsov A.B., Skublov S.G. Geochemical Features of Chondrules from Orlovka Meteorite (H5): Evidence of Melting Precursors. *Doklady Earth Sciences*. 2022. Vol. 504. N 1, p. 254-258. DOI: 10.1134/S1028334X22050166

35. Sukhanova K.G., Kuznetsov A.B., Skublov S.G., Galankina O.L. Evaluation of Thermal Metamorphism Temperature of Equilibrated Ordinary Chondrites. *Geodynamics & Tectonophysics*. 2022. Vol. 13. N 2s, N 0618. DOI: 10.5800/GT-2022-13-2s-0618

36. Yavuz F., Yildirim D.K. A Windows program for calculation and classification of epidote-supergroup minerals. *Periodico di Mineralogia*. 2018. Vol. 87. N 3, p. 269-285. DOI: 10.2451/2018PM808

37. Locock A.J. An Excel spreadsheet to classify chemical analyses of amphiboles following the IMA 2012 recommendations. *Computers & Geosciences*. 2014. Vol. 62, p. 1-11. DOI: 10.1016/j.cageo.2013.09.011

38. Warr L.N. IMA-CNMNC approved mineral symbols. *Mineralogical Magazine*. 2021. Vol. 85. Iss. 3, p. 291-320. DOI: 10.1180/mgm.2021.43

39. McDonough W.F., Sun S.-S. The composition of the Earth. *Chemical Geology*. 1995. Vol. 120. Iss. 3-4, p. 223-253. DOI: 10.1016/0009-2541(94)00140-4

40. Barth T.F.W. Oxygen in Rocks: A Basis for Petrographic Calculations. *The Journal of Geology*. 1948. Vol. 56. Iss. 1, p. 50-60. DOI: 10.1086/625477

41. Langmuir C.H., Vocke Jr.R.D., Hanson G.N., Hart S.R. A general mixing equation with applications to Icelandic basalts. *Earth and Planetary Science Letters*. 1978. Vol. 37. Iss. 3, p. 380-392. DOI: 10.1016/0012-821X(78)90053-5

42. Skublov S.G. Geochemistry of rare earth elements in rock-forming metamorphic minerals. Saint Petersburg: Nauka, 2005, p. 147 (in Russian).

43. Skublov S., Drugova G. Patterns of trace-element distribution in calcic amphiboles as a function of metamorphic grade. *The Canadian Mineralogist*. 2003. Vol. 41. Iss. 2, p. 383-392. DOI: 10.2113/gscanmin.41.2.383

44. Collins W.J., Murphy J.B., Johnson T.E., Hui-Qing Huang. Critical role of water in the formation of continental crust. *Nature Geoscience*. 2020. Vol. 13. Iss. 5, p. 331-338. DOI: 10.1038/s41561-020-0573-6

45. Gieré R. Hydrothermal mobility of Ti, Zr and REE: examples from the Bergell and Adamello contact aureoles (Italy). *Terra Nova*. 1990. Vol. 2. Iss. 1, p. 60-67. DOI: 10.1111/j.1365-3121.1990.tb00037.x

46. Shatskii V.S., Simonov V.A., Jagoutz E. et al. New Data on the Age of Eclogites from the Polar Urals. *Doklady Earth Sciences*. 2000. Vol. 371 A, p. 534-538.

47. Kennett J.P. Marine Geology. Englewood Cliffs: Prentice-Hall, 1982, p. 813.

***Authors*: Laysan I. Salimgaraeva,** *Candidate of Geological and Mineralogical Sciences*, *Junior Researcher*, *fluoritecaf2@mail.ru*, *https://orcid.org/0000-0002-3285-847X* (*Institute of Precambrian Geology and Geochronology RAS*, *Saint Petersburg*, *Russia*; *The Zavaritsky Institute of Geology and Geochemistry*, *Ural Branch of the RAS*, *Ekaterinburg*, *Russia*), **Alexei V. Berezin,** *Candidate of Geological and Mineralogical Sciences*, *Senior Researcher*, *Associate Professor*, *https://orcid.org/0000-0002-5324-5840* (*Institute of Precambrian Geology and Geochronology RAS*, *Saint Petersburg*, *Russia*; *Institute of Earth Sciences*, *Saint Petersburg State University*, *Saint Petersburg*, *Russia*).

The authors declare no conflict of interests.

This is an open access article under the CC BY 4.0 license